On-Chip Slow-Light SiN Bragg Grating Waveguides

Alexander Chen, *Graduate Student Member, IEEE*, Amir Begović, *Graduate Student Member, IEEE*, Stephen Anderson, *Graduate Student Member, IEEE*, and Zhaoran Rena Huang, *Member, IEEE*

***Abstract*—Si photonic foundry fabricated cascaded and continuous spiral shaped silicon nitride (SiN) waveguides that incorporate Bragg grating structures were explored to produce an on-chip true-time delay line. A time-domain measurement method was used to characterize the delay time of the grating waveguides near their photonic band edge where it exhibits the strongest slow light effect. The highest group index extracted from cascaded SiN grating waveguides is 19.7 corresponding to a total delay time of 5.48 ns in a full length of 12.49 cm that consumes a surface area of 2.66 mm^2. A continuous spiral SiN grating waveguide was also fabricated which produces a delay time of 3.78 ns in a length of 5.47 cm with a surface area consumption of 0.88 mm^2.**

***Index Terms*—Silicon nitride, Bragg gratings, slow light.**

I. Introduction

OPTICAL true time delay line is a critical component in many optical systems such as optical signal buffers [1], [2], optical frequency combs [3], photonic beamforming [4], [5], and optical signal processing [6], [7]. Depending on the application, the required delay time can range from picoseconds to tens of nanoseconds. By adjusting the fiber length, a single mode optical fiber (unit delay of approximately 4.9 μs/km [8]) is widely used to produce the appropriate delay time in optical systems. In the last few years, several Si photonic foundries [9], [10] were established and many efforts were made to transfer assembled discrete optical systems to chip-scale optoelectronic microsystems on a Si platform that offers much improved size, weight and power (SWaP) efficiency.

It is a challenge to produce long delay lines on Si chips. Si nanowire waveguides, with typical group indices of approximately 4.2 [11], give a unit time delay of 0.14 ns/cm. Other devices have been studied to achieve large time delays.

Coupled Resonator Optical Waveguides (CROWs) have been explored for delay line applications. Ferrari et al. [12] reported 550 ps of delay using 50 coupled resonators on a central optical waveguide. The drawback of CROWs is that any imperfections within the CROW will negatively affect the effective delay experienced by the optical pulse. In addition, the high Q factor increases photon lifetime, thus decreasing the bandwidth.

Manuscript received 5 October 2022; revised 2 November 2022; accepted 3 November 2022. Date of publication 8 November 2022; date of current version 2 December 2022. This work was supported in part by U.S. Air Force Research Lab (AFRL) in Rome, NY under Grant FA8750-16-3-6003 and in part by SMART Scholar Program under Grant W911NF-22-2-0156. *(Corresponding author: Zhaoran Rena Huang.)*

The authors are with the Rensselaer Polytechnic Institute (RPI), Troy, NY 12180 USA (e-mail: chena12@rpi.edu; begova@rpi.edu; anders8@rpi.edu; huangz3@rpi.edu).

Digital Object Identifier 10.1109/JPHOT.2022.3220540

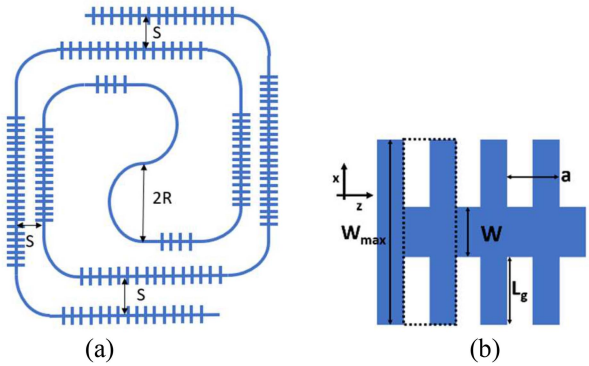

Fig. 1. (a) A schematic of the cascaded spiral grating (not to scale). All curved portions are plain waveguides while all straight portions are grating waveguides with an apodization profile applied. The number of grating segments range from 42 to 122 total grating segments. (b) A schematic of the top view of a Bragg grating waveguide. The optical wave travels along the z-direction. The SiN film thickness is measured in the y-direction. A dashed box outlines the unit cell of the grating.

Utilizing traveling wave resonance along its propagation direction is another approach to achieve increased on-chip delay time. Defect engineered photonic crystal waveguides (PhW) have reported high group indices (20–90) within a spectrum range of approximately 4.5 nm [13]. Fabrication of these line defect engineered PhW at the desired accuracy and repeatability is a challenge in Si foundries. Under strong slow light, PhW also exhibits drastically increased propagation loss due to enhanced scattering loss [14].

Bragg gratings incorporated in a waveguide can be considered as a one-dimensional periodic dielectric structure [15]. The sidewall corrugations induce a moderate optical field slow-light effect. Comparing to the circularly shaped, plasma etched through-holes in PhW, the rectangularly shaped Bragg grating is easier to fabricate and has a high tolerance to fabrication offsets that can vary across the chip. For example, the corner of the rectangular grating bar often appears to be rounded during fabrication, resulting in quasi-sinusoidal shaped corrugations, whereas the bandgap properties are only moderately affected by these fabrication constraints, which does not hold for PhW.

Slow-light effect in Si grating waveguide and its applications for true-time delay lines have already been studied [16], [17], [18]. SiN/SiO_2 waveguide on SOI substrate has demonstrated up to several orders of propagation loss reduction [19], [20], [21], [22], [23] and low loss SiN waveguides have been widely used to produce on-chip optical delay lines [24], [25]. For example, Moreira et al. [26] reported a SiN waveguide with a time delay of 12.35 ns and propagation loss of 1 dB/m. However, SiN gratings

for delay lines have not been thoroughly characterized. Due to stresses arising from the differences in thermal expansion between the SiN film and the substrate leading to cracks and rendering the film optically unusable [27], [28], [29], the SiN film thickness is often limited to <400 nm resulting in a large portion of the optical mode traveling in the cladding layer. In this work, we utilize American Institute of Manufacturing Photonics (AIM Photonics) foundry for SiN waveguide fabrication. The SiN layer at AIM has a thickness of 220 nm which gives an effective index of 1.6. The weaker optical field confinement leads to a stronger slow light effect due to increased sidewall corrugation interaction. This work intends to systematically study SiN/SiO_2 grating perturbation strength in relation with group index and propagation loss. The effects of a cascaded delay line versus a continuous delay line will also be studied in this work.

II. Device Structures and Theoretical Analysis

A. Spiral SiN Grating Waveguides

A schematic of a Bragg grating waveguide is shown in Fig. 1 that labels the waveguide width *W*, grating side bar length L_g, total grating waveguide width $W_{\max,}$ and period *a*. The duty cycle is the ratio of corrugation width to the period *a*.

Spiral grating waveguides were designed to produce long delay times on chip. As shown in Fig. 1, the inner bends of all spiral waveguides have a bending radius R = 120 μm and the center-to-center separation between two adjacent waveguides is S = 20 μm. The grating elements are held in the straight portion of the spiral while the curved portion is a quarter circle of plain waveguide. An outward super-Gaussian apodization profile was applied to the grating structure to suppress side band oscillation. The apodized grating also provides better mode matching between the plain waveguide to slow-light waveguide [30]. The modulation profile follows

$$f\ (x) = \exp\left(-\frac{1}{2}\left(\frac{\frac{x}{L} - 0.5}{\alpha}\right)^n\right)\ , \tag{1}$$

where L is the length of the structure, n is the order of the super-Gaussian profile, and α is the full maximum at half width of the function. The choice of n and α affect the performance of the device. Smaller n and α lead to a smoother index transition from the plain waveguide to the grating waveguide segment; group index is sacrificed in favor of an enhanced index matching device and more efficient suppression of side band oscillations [31]. In this work, n = 8 and α = 0.39 are chosen.

B. Device Fabrication

Seven cascade spiral grating samples (A to G) were fabricated in a multi-project wafer (MPW) passive run while a continuous grating spiral, Sample H, was patterned in the SiN layer of an active MPW run next to Si active devices such as Si modulators and photodetectors. To maintain a single mode operation, the maximum waveguide width of the SiN waveguide is 1.5 μm for TE polarization. We evaluated multiple waveguide widths, 850 nm, 950 nm, 1100 nm and 1250 nm, to have a transverse mode diameter calculated at 1/e of the electric field magnitude of 1.25 μm, 1.27 μm, 1.34 μm, and 1.42 μm, respectively. Vertical mode diameter is approximately 0.9 μm and varies slightly with SiN width choice. The grating period *a* is 495 nm except Sample A with *a* = 500 nm and Sample H with *a* = 498 nm. The variation of period in a small range leads to a spectrum shift of the photonic band edge of the same band, providing a method to tune the slow light operating wavelengths at a designated spectrum location. Sample parameters are summarized in Table I. All devices have a duty cycle of 50%. In Table I, *L* is the total length of the grating spiral waveguide.

TABLE I
Grating Parameters

	W (nm)	W_{max} (nm)	a (nm)	L (cm)	Surface Area (mm^2)
A	950	1600	500	7.00 cm	1.54 mm^2
B	1100	1600	495	4.05 cm	0.91 mm^2
C	1250	1600	495	12.49 cm	2.66 mm^2
D	850	2200	495	12.49 cm	2.66 mm^2
E	950	2200	495	12.49 cm	2.66 mm^2
F	1100	2200	495	12.49 cm	2.66 mm^2
G	1250	2200	495	3.04 cm	0.7 mm^2
H	950	1500	498	5.47 cm	0.88 mm^2

C. Photonic Band Structure

Group velocity (v_g) quantifies the energy packet of an optical signal traveling in a medium that can be at a slower speed than the wavefront phase velocity. Group index (n_g) is defined as the ratio of group velocity to the speed of light c:

$$n_g = \frac{c}{v_g}\ . \tag{2}$$

In a dispersive waveguide, the group index can be described by [8]

$$n_g = n_{eff}\ + \omega\frac{\partial n_{eff}}{\partial \omega}, \tag{3}$$

where n_{eff} is the effective modal index of the waveguide and ω is the optical frequency. For the SiN waveguide with a width of 1 μm, n_{eff} is approximately 1.6 for TE polarization. The material dispersion of SiN near c-band is small so the perturbation of the grating accounts for the increased n_g.

A Bragg grating waveguide can be analyzed by photonic crystal waveguide theory. The photonic band diagrams in Fig. 2 were generated using a frequency-domain simulator that solves for the eigenstates and eigenvalues of Maxwell's equations for the lowest 5 TE bands. The unit cell used in the simulation is depicted in the dashed box of Fig. 1(b). In the wavelength range of 1456 nm to 1547 nm, the 0th and 1st order photonic band gaps are identified. All samples exhibit similar band diagrams, and a representative band diagram of Sample D is plotted in Fig. 2. The 0th order band has a wider band gap, suggesting a stronger slow light effect than the 1st order band. Therefore, in this work, we focus on slow light regime in the 0th order band edge.

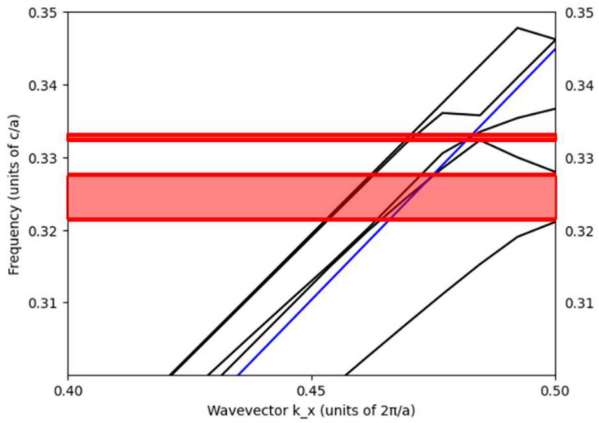

Fig. 2. Simulated photonic band diagram for Sample D. The blue line represents the light line in oxide, the red regions indicate the 0th and the 1st photonic band gaps. The photonic band diagrams for other samples are very similar to sample D.

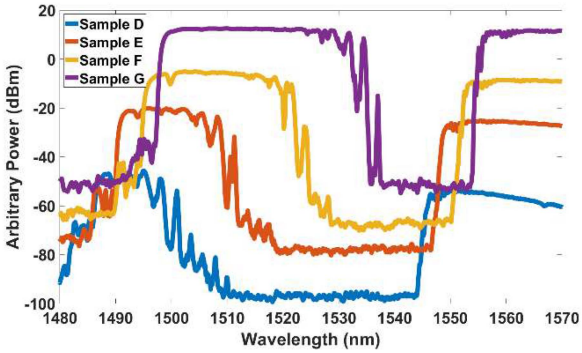

Fig. 3. The relative transmitted optical power for samples D, E, F and G. The output optical powers of these 4 samples are plotted with 10 dB difference for graph clarity. The slow light region that is used to produce the delay-line is circled in the graph.

III. Device Characterization and Results Discussion

We first studied Bragg grating waveguide transmission characteristics, then used a time domain method to measure the delay time of all samples, and finally extracted their group indices.

A. Device Transmission

Plotted in Fig. 3, we first measured Samples D to G to study how the waveguide width W impacts the transmission spectra. All samples exhibit a photonic band gap in the c-band near 1550 nm as designed. The effective index n_{eff} varies due to different Bragg grating waveguide geometry, resulting in a shift of the band gap location. The grating bar length L_g follows a super-Gaussian apodization function to suppress side band oscillations [30]. The stop band width in the transmission spectra suggests the relative slow light strength among samples and they are listed in Table II. Sample D with the smallest waveguide width $W = 850$ nm and the longest grating bar width $W_{\max} = 2.2$ μm has the strongest slow light effect among Samples D to G.

TABLE II
Grating Delay Time and Propagation Loss

	λ (nm) at band edge	n_g	Delay/ Length (ns/cm)	Slow Light Propagation Loss (dB/cm)	Stop Band Width (nm)
A	1550	9.8	0.33	2.29	18.2
B	1540	9.2	0.31	2.08	10.9
C	1543	8.7	0.29	1.78	7.66
D	1545	n/a	n/a	3.82	37.5
E	1548	19.7	0.56	2.44	30.6
F	1552	12.2	0.41	2.24	23.9
G	1555	11.3	0.38	1.97	17.8

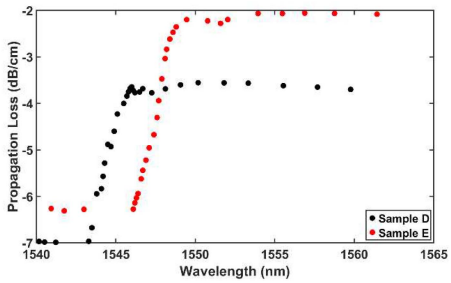

Fig. 4. Propagation loss near the band edge of sample D and sample E. There is a trade-off between slow light strength and loss.

B. Propagation Loss Characterization

An increased propagation loss is the trade-off to stronger slow light effect for these traveling wave resonant structures. An edge coupler, provided by AIM PDK, is used in both the input and output ends of a cascaded spiral waveguide that has a measured insertion loss of 2.9 dB/facet. The propagation loss of the spiral grating waveguides is measured using different lengths of waveguides and then calculating the best fit line. The facet-to-chip coupling loss, the propagation loss in the grating and plain waveguide segments, bending loss, and modal coupling loss at the grating segment and plain waveguide interface all contribute to the total insertion loss. With a bending radius of 120 μm, the SiN waveguide bending loss is negligible [32], [33], confirmed by our simulated results. The simulated reflection due to mode mismatch from plain waveguide to the apodized grating is approximately 0.03 dB. The scattering loss due to enhanced wave-matter interaction in the slow-light region is the dominant waveguide propagation loss.

For all samples, the propagation loss increases near the band edge due to increased slow light effect. Using Samples D and E as an example, we plotted the device propagation loss varying with wavelength, shown in Fig. 4. Sample E shows a baseline propagation loss of 2.18 dB/cm outside the slow light region. Sample D is expected to have the strongest slow light effect at the price of increased propagation loss when compared to Samples E to G. It shows a baseline propagation loss of 3.98 dB/cm, too high to obtain meaningful delay time measurement for the current spiral SiN design and was excluded from the delay time test.

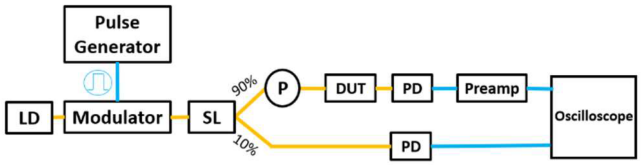

Fig. 5. A schematic of the delay line test setup. Optical paths are in yellow, and the electrical paths are in blue. A Keysight tunable laser (symbol LD) with 5 pm of wavelength tuning resolution was used. SL represents a splitter that has a 90:10 splitting ratio and P represents a polarizer.

C. Delay Time Characterization

The wavelength dependent time delay of the SiN spirals was characterized by a true-time delay setup, as shown in Fig. 5. An electrical pulse 270 ps in width was generated to drive a high-speed optical intensity modulator (Optilab IM-1550-20-A). The modulated signal passes through a 90:10 splitter to two paths, namely the SiN waveguide path and the reference optical path. A pre-amplifier with 25 dB gain is placed in the SiN waveguide path to boost the signal level for measurement. The pulses from both paths are displayed simultaneously on a sampling oscilloscope (Agilent 83484A). The test setup was carefully calibrated to take account of the jitter of various electrical components and extra time delays caused by the fibers and connectors. The time delay data of the SiN spiral was exported from the oscilloscope and examined via cross-correlation method in post processing.

Delay time versus wavelength is characterized near the band edge within a 10 nm range. As the optical test path has a much higher loss than the reference path, the detected optical signal from the SiN waveguide path is weak with distorted pulse shape that lowers the accuracy in the pulse cross-correlation calculation. The chirp caused by the grating structure can further widen and distort the pulse shape. A two-termed exponential curve is fitted to the data for analysis. Increased data density was applied near the band edge. Within 100 pm from the stopband edge, data was taken with a step size of 10 pm. Up to 1 nm, 3 nm and 10 nm from the band edge, data was taken in a step of 100 pm, 500 pm and 1 nm, respectively. Group indices were extracted from the measured time delay data near the photonic band edge. As the grating geometry (W, $W_{\max}$, a) is different among all the samples, the photonic band edge varies as well. Fig. 6 plots the group index n_g for all samples with an artificial wavelength shift for easier comparison.

Samples E, F, and G have similar grating waveguide structures but different center waveguide width. A stronger slow light effect is anticipated in a smaller waveguide width. Sample E with $W = 950$ nm exhibited the largest $n_g = 19.7$ at $\lambda = 1540$ nm near the band edge, leading to an on-chip time delay of 8.2 ns in an area of 2.66 mm^2. To the best of our knowledge, it is the longest on-chip time delay reported.

Besides the waveguide core width, the Bragg grating side bar length L_g also impacts the optical field perturbation strength. A large L_g may induce higher order modes in the Bragg waveguide. Sample A and E has L_g length of 325 nm and 625 nm, respectively, and their simulated transverse profiles are plotted in Fig. 7. An extended transverse mode profile leads to stronger

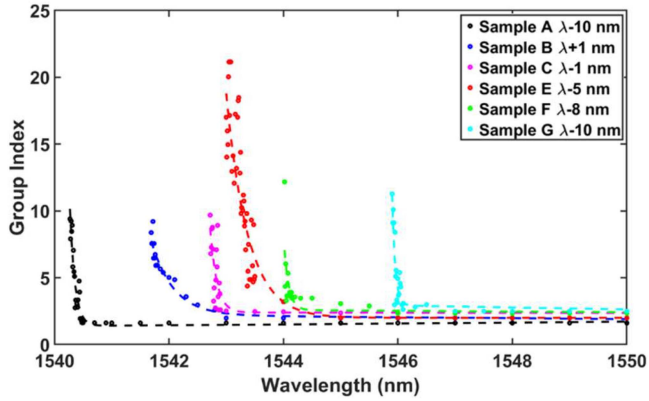

Fig. 6. A comparison of the extracted group index for samples A, B, C, E, F, and G. Artificial wavelength shift is applied on samples for the plot's clarity. For example, sample A's band edge was measured at around 1550 nm but is shifted to 1540 nm and marked as $\lambda - 10$ nm in the legend.

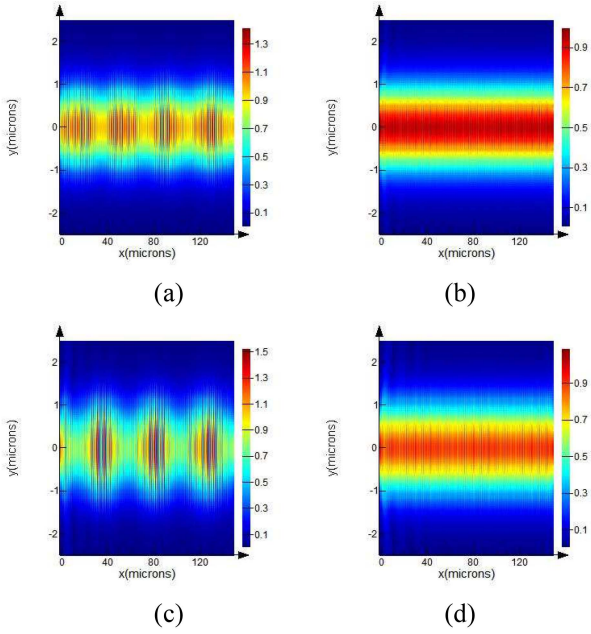

Fig. 7. Electric field profile of light traveling in the Bragg waveguide for Sample A in (a) and (b) and Sample E in (c) and (d). (a) and (c) plot the mode profile in a slow light wavelength regime while (b) and (d) are outside slow light wavelength regime.

field interaction with the grating corrugation. In the slow light region, a standing wave is clearly noticeable compared to the wave propagation outside the slow-light region. Sample E has demonstrated much larger group index than that of Sample A. Comparing Sample B with F, C with G, a similar slow light effect difference is observed. Table II summarizes the highest group index of each waveguide obtained at the wavelength listed in the second column and their corresponding propagation loss.

In a standard Si foundry such as AIM Photonics, Si nanowire waveguide is reported to have a propagation loss of 2.2–2.5 dB/cm in the 1500–1550 nm range [19]. Using $n_g = 4.2$ [34] in Si waveguide spiral, we estimate a unit length delay time of 0.14 ns/cm. As a comparison, Samples E and F have a similar unit length loss, $<$2.5 dB/cm, but can offer a much larger unit length

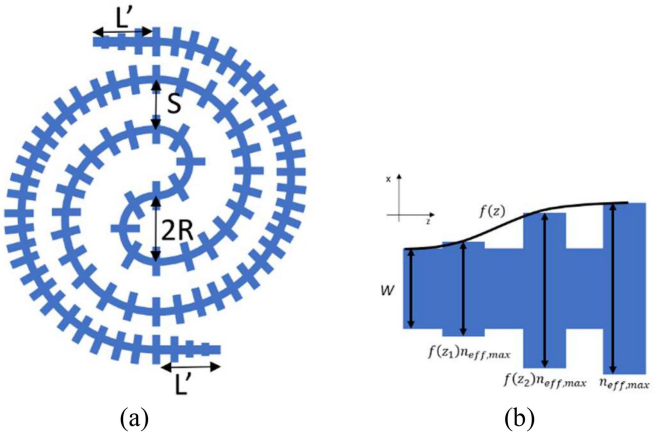

Fig. 8. (a) Schematic of a continuous grating spiral with the apodized tail ends. Bending radius R is 120 μm and separation distance S is 10 μm. (b) The assumption used in the transfer matrix method to account for the apodization profile.

time delay of 0.56 and 0.41 ns/cm, respectively. Sample C has a group index approximately 2 times greater than Si waveguide while displaying a loss of 1.78 dB/cm, lower than a typical Si waveguide.

D. Cascade Bragg Grating Transmission

Samples A to G are cascaded gratings that consist of grating segments of decreasing length going into the spiral and increasing length leaving the spiral connected by curved plain waveguide segments of bending radius R = 120 μm, as seen in Fig. 1(a). We anticipate a strong filter effect from these cascaded grating spirals. We also characterized Sample H which is a circular spiral with continuous grating perturbations throughout the delay waveguide, shown in Fig. 8(a). As the core waveguide has a curvature, the grating bar orientation varies and is situated such that the grating bars are always normal to the tangent line to the curve. The designed grating spiral parameters are W = 950 nm, $W_{\max}$= 1.5 μm, a = 498 nm, and length of 5.2 cm and no apodization is applied to the grating bar width over the spiral. A straight portion of SiN grating waveguide with a length of 249 μm and half of a super-Gaussian apodized profile is placed at both ends of the continuous spiral. Overall, there are 23 turns in the grating spiral. The total length of the SiN grating waveguide is 5.47 cm.

Both Samples A and H have demonstrated good suppression of side-band oscillation experimentally, and Sample H, shown in Fig. 9, has shown slightly less transmission ripples than that of Sample A. The super-Gaussian function changes more gradually in the continuous grating spiral than that of the grating pieces of the cascade spiral, providing better impedance match at the interface leading to less power ripples in the transmission spectrum.

The total delay time measured per unit length for Sample A and H are plotted in Fig. 10. The cascaded grating structure of Sample A has exhibited a strong filter effect as the spectrum pass band with strong slow light only spans approximately 0.5 nm. Sample H has a gradual delay time/unit length variation

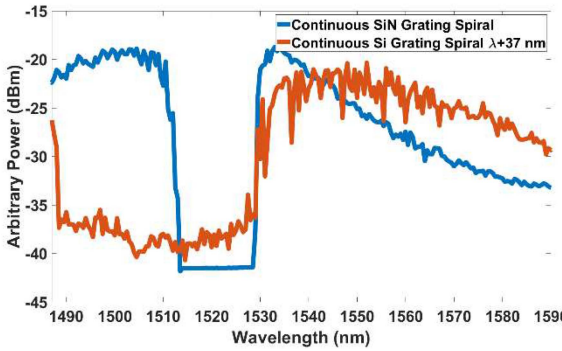

Fig. 9. Transmission spectra of the continuous SiN grating spiral and the continuous Si grating spiral. The response of the vertical grating coupler has not been considered.

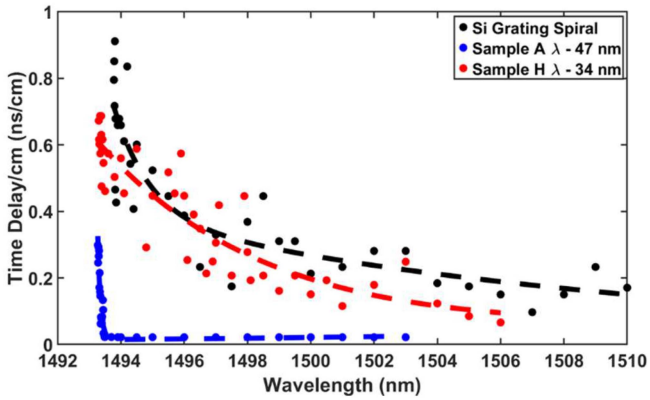

Fig. 10. Time delay per unit length of a Si grating spiral versus sample A versus sample H. Instead of an optical in and optical out setup as shown in Fig. 6, the optical out of the Si grating spiral and sample H is replaced with an on-chip PD.

with wavelength across >10 nm range. We also utilized matrix formulation method to model the transmission of Sample A and H, and Sample A has a wider stop band suggesting potentially a stronger slow-light effect. However, in practice it is difficult to tune the laser wavelength to match exactly the strong slow light wavelength of the cascaded grating, so experimentally, Sample H has shown higher time delay/unit length. For on-chip true-time delay line application, continuous spiral grating waveguides, though more complex in layout generation, can produce stronger slow light in a wider spectrum regime with relaxed wavelength alignment requirement.

A Si spiral with continuous grating corrugation was also fabricated on the same MPW run as Sample H. The Si grating spiral has a center waveguide width of W = 400 nm, $W_{\max}$ = 800 nm, a = 306 nm, L = 2 cm, a minimum bending radius R = 35 μm, and a separation distance S = 9 μm. The delay time testing results are also plotted in Fig. 10. In our measurement, the highest delay/length for SiN and Si spiral grating waveguide are 0.7 ns/cm and 0.95 ns/cm, respectively, measured at the highest group delay. A comparison in surface area and propagation loss trade-off between the SiN and Si grating spirals are summarized in Table III where the delay time/area is calculated based on generating 5 ns of time delay in both structures. As expected,

TABLE III
SiN AND Si GRATING SPIRAL WAVEGUIDE COMPARISON

	Delay per Length (ns/cm)	Delay per Area (ns/mm^2)	Loss per Delay (dB/ns)
SiN	0.7	5.7	5.43
Si	0.95	20.8	10.42

the Si grating spiral exhibits a larger unit length delay while encountering higher propagation loss. A considerable propagation loss difference to produce a unit time delay is observed.

IV. CONCLUSION

Using a Si foundry processing line, SiN spiral grating waveguides were fabricated with varying waveguide grating geometry and their unit time delay and propagation loss are characterized experimentally. The strongest slow light effect was observed in cascaded grating spiral with parameters of $W = 950$ nm, $W_{\max} = 2.2$ μm, $a = 495$ nm, and $L = 12.49$ cm producing a unit time delay of 0.56 ns/cm at the cost of high propagation loss of 2.44 dB/cm.

A grating spiral with continuously changing radius was also designed and fabricated on SiN and Si layer using AIM foundry service. Comparing the SiN multi-segment grating spiral with the continuous spiral grating waveguide, the slow light effect in the continuous grating spiral is evident in a wider spectrum, approximately 10 nm, while a strong filter effect is observed on the multi-segmented grating spiral. The SiN continuous grating spiral demonstrates a unit time delay of 0.7 ns/cm, a total on-chip delay of 3.83 ns and propagation loss merit of 5.43 dB/ns. The Si grating spiral unit time delay and propagation loss are also characterized experimentally, and a trade-off between surface area consumption and loss per unit delay time are observed.

ACKNOWLEDGMENT

The authors would like to thank AFRL and AIM Photonics for chip space on the Venom and Nye run, respectively.

REFERENCES

[1] R. W. Boyd, D. J. Gauthier, and A. L. Gaeta, "Applications of slow light in telecommunications," *Opt. Photon. News*, vol. 17, no. 4, pp. 18–23, 2006.
[2] K. Takiguchi, M. Itoh, and T. Shibata, "Optical-signal-processing device based on waveguide-type variable delay lines and optical gates," *J. Lightw. Technol.*, vol. 24, no. 7, pp. 2593–2601, Jul. 2006.
[3] H. Tian et al., "Optical frequency comb noise spectra analysis using an asymmetric fiber delay line interferometer," *Opt. Exp.*, vol. 28, no. 7, pp. 9232–9243, 2020.
[4] S. Anderson, A. Begovic, A. Chen, Z. R. Huang, W. Zhou, and G. Sun, "Integrated silicon photonic true-time delay beam-former for wide-band phased-array antenna," in *Proc. IEEE 70th Electron. Compon. Technol. Conf.*, 2020, pp. 162–167.
[5] J. Capmany, B. Ortega, and D. Pastor, "A tutorial on microwave photonic filters," *J. Lightw. Technol.*, vol. 24, no. 1, pp. 201–229, Jan. 2006.
[6] F. Duport, B. Schneider, A. Smerieri, M. Haelterman, and S. Massar, "All-optical reservoir computing," *Opt. Exp.*, vol. 20, no. 20, pp. 22783–22795, 2012.
[7] L. Appeltant et al., "Information processing using a single dynamical node as complex system," *Nature Commun.*, vol. 2, no. 1, pp. 1–6, 2011.
[8] S. O. Kasap, *Optoelectronics and Photonics: Principles and Practices*, 2nd ed. London, U.K.: Pearson Int., 2013.
[9] AIM photonics, 2022. [Online]. Available: https://www.aimphotonics.com/
[10] IMEC, 2022. [Online]. Available: https://www.imec-int.com/en/integrated-photonics
[11] L. Chrostowski and M. Hochberg, *Silicon Photonics Design*. Cambridge, U.K.: Cambridge Univ. Press, 2015.
[12] C. Ferrari, F. Morichetti, and A. Melloni, "Disorder in coupled-resonator optical waveguides," *J. Opt. Soc. Amer. B*, vol. 26, pp. 858–866, 2009.
[13] M. Notomi, K. Yamada, A. Shinya, J. Takahashi, C. Takahashi, and I. Yokohama, "Extremely large group-velocity dispersion of line-defect waveguides in photonic crystal slabs," *Phys. Rev. Lett.*, vol. 87, no. 25, 2001, Art. no. 253902.
[14] L. O'Faolain, T. P. White, D. O'Brien, X. Yuan, M. D. Settle, and T. F. Krauss, "Dependence of extrinsic loss on group velocity in photonic crystal waveguides," *Opt. Exp.*, vol. 15, no. 20, pp. 13129–13138, 2007.
[15] J. D. Joannopoulos, S. G. Johnson, J. N. Winn, and R. D. Meade, *Photonic Crystals: Molding the Flow of Light*. Princeton, NJ, USA: Princeton Univ. Press, 2008.
[16] M. L. Povinelli, S. G. Johnson, and J. D. Joannopoulus, "Slow-light, band-edge waveguides for tunable time delays," *Opt. Exp.*, vol. 13, no. 18, pp. 7145–7159, 2005.
[17] F. Riboli, P. Bettotti, and L. Pavesi, "Band gap characterization and slow light effects in one dimensional photonic crystals based on silicon slot-waveguides," *Opt. Exp.*, vol. 15, no. 19, pp. 11769–11775, 2007.
[18] C.-J. Chung, X. Xu, G. Wang, Z. Pan, and R. T. Chen, "On-chip otpical true time delay lines featuring one-dimensional fishbone photonic crystal waveguide," *Appl. Phys. Lett.*, vol. 112, no. 7, 2018, Art. no. 071104.
[19] A. Photonics, "APSUNY process development kit full-build component library documentation," *AIM-Photon.*, early access, 2020.
[20] R. Baets et al., "Silicon photonics: Silicon nitride versus silicon-on-insulator," in *Proc. Opt. Fiber Commun. Conf. Exhib.*, 2016, pp. 1–3.
[21] J. F. Bauters et al., "Planar waveguides with less than 0.1 dB/m propagation loss fabricated with wafer bonding," *Opt. Exp.*, vol. 19, no. 24, pp. 24090–24101, 2011.
[22] J. F. Bauters et al., "Ultra-low-loss high-aspect-ratio Si_3N_4 waveguides," *Opt. Exp.*, vol. 19, no. 4, pp. 3163–3174, 2011.
[23] K. Luke, A. Dutt, C. B. Poitras, and M. Lipson, "Overcoming Si_3N_4 film stress limitations for high quality factor ring resonators," *Opt. Exp.*, vol. 21, no. 19, pp. 22829–22833, 2013.
[24] B. Sharma, K. Kishor, A. Pal, S. Sharma, and R. Makkar, "Design and simulation of ultra low loss spiral delay line for integrated optical coherence tomography," *Opt. Quantum Electron.*, vol. 53, no. 7, pp. 1–13, 2021.
[25] D. Bykhovsky, M. Rosenblit, and S. Arnon, "Two-sided through-wafer interconnect for optical spiral delay line," *J. Modern Opt.*, vol. 65, no. 1, pp. 98–103, 2018.
[26] R. L. Moreira et al., "Integrated ultra-low-loss 4-bit tunable delay for broadband phased array antenna applications," *IEEE Photon. Technol. Lett.*, vol. 25, no. 12, pp. 1165–1168, Jun. 2013.
[27] J. S. Levy, *Integrated Nonlinear Optics in Silicon Nitride Waveguides and Resonators*. Ithaca, NY, USA: Cornell Univ. Press, 2011.
[28] D. R. Southworth et al., "Stress and silicon nitride: A crack in the universal dissipation of glasses," *Phys. Rev. Lett.*, vol. 102, no. 22, 2009, Art. no. 225503.
[29] K. H. Nam, I. H. Park, and S. H. Ko, "Patterning by controlled cracking," *Nature*, vol. 485, pp. 221–224, 2012.
[30] S. Khan and S. Fathpour, "Demonstration of complementary apodized cascaded grating waveguides for tunable optical delay lines," *Opt. Lett.*, vol. 38, no. 19, pp. 3914–3917, 2013.
[31] L. Jiang and Z. R. Huang, "Integrated cascaded Bragg gratings for on-chip optical delay lines," *IEEE Photon. Technol. Lett.*, vol. 30, no. 5, pp. 499–502, Mar. 2018.
[32] M. J. R. Heck, J. F. Bauters, M. L. Davenport, D. T. Spencer, and J. E. Bowers, "Ultra-low loss waveguide platform and its integration with silicon photonics," *Laser Photon. Rev.*, vol. 8, no. 5, pp. 667–686, 2014.
[33] L. Wang, W. Xie, D. Van Thourhout, Y. Zhang, H. Yu, and S. Wang, "Nonlinear silicon nitride waveguides based on a PECVD deposition platform," *Opt. Exp.*, vol. 26, no. 8, pp. 9645–9654, 2018.
[34] I.-W. Hsieh et al., "Cross-phase modulation-induced spectral and temporal effects on co-propagating femtosecond pulses in silicon photonic wires," *Opt. Exp.*, vol. 15, no. 3, pp. 1135–1146, 2007.